On the structure of polaronic defects in thiophene oligomers: A combined Hartree–Fock and Density Functional Theory study

ARTICLE *in* SYNTHETIC METALS · JANUARY 2000

Impact Factor: 2.25 · DOI: 10.1016/S0379-6779(99)00287-8

4 AUTHORS, INCLUDING:

Giorgio Moro
Università degli Studi di Milano-Bicocca
60 PUBLICATIONS **1,057** CITATIONS
SEE PROFILE

Giovanni Scalmani
Gaussian, Inc.
82 PUBLICATIONS **9,440** CITATIONS
SEE PROFILE

Pitea Demetrio
Università degli Studi di Milano-Bicocca
135 PUBLICATIONS **1,520** CITATIONS
SEE PROFILE

ELSEVIER

Synthetic Metals 108 (2000) 165–172

SYNTHETIC METALS

www.elsevier.com/locate/synmet

On the structure of polaronic defects in thiophene oligomers: a combined Hartree–Fock and Density Functional Theory study

Giorgio Moro *, Giovanni Scalmani [1], Ugo Cosentino, Demetrio Pitea

Dipartimento di Chimica Fisica ed Elettrochimica, Università degli Studi di Milano, via C. Golgi, 19, 20133 Milan, Italy

Received 23 June 1999; received in revised form 19 October 1999; accepted 3 November 1999

Abstract

Thiophene oligomer radical cations were studied as model for the polaronic defects in doped polythiophenes. Oligomers of increasing size (2 to 10 rings) were characterized by means of ab initio calculations. Optimized geometries and charge distributions were computed at both the Hartree–Fock (HF) and Density Functional Theory (DFT) levels. When electron correlation is taken into account the whole shape of the polaronic defect changes so that the self-localization of the positive charge and the corresponding quinoid structural distortion are greatly reduced. The energetics of the aromatic vs. quinoid geometry is investigated using substituted bithiophenes as model compounds. The discrepancy between HF and DFT results is confirmed. Traditional post-HF approach is found to agree with DFT.

Keywords: Oligothiophenes; Ab initio quantum chemistry methods and calculations; Density Functional Theory calculations

1. Introduction

The thorough understanding of the electrical conduction phenomena in doped conjugated organic polymers (polythiophene, polypirrole, poly-*p*-phenylene, etc.), is a step of fundamental importance towards the design of new electronic and electro-optical devices [1,2]. Unfortunately, the characterization of the physico-chemical properties and the disclosure of the microscopical morphology of this class of polyconjugated systems is often difficult because of their limited stability and processibility [3].

In the last few years, researchers have focused their attention not only on polymers made through electropolymerization, but also on the synthesis of oligomers with controlled structure and length. These oligomers can be more easily isolated, characterized and handled. The oligomer's molecular structure can be finely tailored by controlling the number of rings. Moreover, their physico-chemical properties (solubility, oxidation potential, etc.) can be modified by the presence of substituents with different stereoelectronic characteristics.

Recently, research efforts focused on oligothiophenes *n*T (*n* = number of rings). The increase in solubility, which can be attained by grafting alkyl chains onto oligothiophenes, allows for direct characterization of neutral and oxidized species in solution by means of spectroscopical techniques [4]. Among the redox states of oligothiophenes, the doubly charged one can be seen as a molecular model for the bipolaron which is believed to be the prevalent form of charge storage in doped polythiophenes, on the basis of both experimental evidences [5,6] and theoretical studies [7–9]. Other redox states of oligothiophenes in solutions have been identified and characterized. Among these, singly charged oligomers [10] and doubly charged π-dimers [11] attract most of the interest, but even more exotic species such as two polarons on a single chain [12], triply charged oligomers [13] and fourfold charged π-dimers have been observed [14].

The amount of information now available from high-quality spectroscopic investigation of oxidized solutions of oligothiophenes has renewed the debate on the actual importance of doubly charged defects (bipolarons) for the rationalization of the electrical and optical response phenomena in doped polythiophenes. Hill et al. [15] and Zinger et al. [16] showed that the experimental evidences

* Corresponding author. Fax: +0039-2-70638129; e-mail: giorgio.moro@unimib.it

[1] Current address: Service de Chimie des Matériaux Nouveaux, Centre de Recherche en Electronique et Photonique Moléculaires, Université de Mons-Hainaut, Place du Parc 20, B-7000 Mons, Belgium.

0379-6779/00/$ - see front matter
PII: S0379-6779(99)00287-8

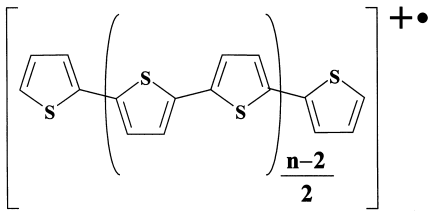

Fig. 1. Molecular structure of the α-oligothiophene radical cations ($n\mathrm{T}^{+\cdot}$) considered in this work.

usually invoked to support the presence of doubly charged oligothiophenes in solutions, can be explained also by the formation of π dimers and stacks. Yokonuma et al. [17] and Furukawa [18] revised the usual interpretation of UV–VIS and Raman spectra of doped polythiophene. They used for comparison the spectroscopic signatures of neutral, singly charged and doubly charged sexythiophene (6T) in solution and concluded that the charge defects in polythiophenes are more likely to be singly charged polarons rather than bipolarons. Recently, van Haare et al. investigated thoroughly the optical properties of 6T, 9T and 12T in solution during the oxidation process [12].

The aim of this work is to contribute to understand the electronic and structural characteristics of singly charged oligothiophenes. By means of ab initio quantum chemical methods, we studied the geometric structure and charge distribution of thiophene oligomer radical cations $n\mathrm{T}^{+\cdot}$ ($n = 2$, 4, 6, 8 and 10, Fig. 1). In particular, we focused our attention on the degree of charge localization and on the extent of the quinoidic structural distortion. As we did in our previous study on doubly charged oligomers [19], we compare results from Hartree–Fock (HF) and Density Functional Theory (DFT) and discuss the electron correlation effects as taken into account by the latter method. Furthermore, we investigate the energetics of aromatic vs. quinoid geometry in a neutral substituted bithiophenes (2T) by means of different theoretical approaches (HF, DFT and more traditional correlated methods like Møller–Plesset perturbation theory, MP2). In fact, according to the theoretical description of charge defects in conjugated systems [7], the energy difference between the aromatic and the quinoid geometry of the neutral chain, is an important factor to establish the spatial extension of both neutral and charged defects.

2. Methods

Open shell systems are usually described by means of unrestricted wave functions which allow each alpha molecular orbital to be different from the corresponding beta one, thus taking into account a certain amount of the electron correlation through spin polarization. However, unrestricted wave functions are not eigenfunctions of the S^2 operator and thus they may suffer from spin contamination by higher spin states. The reliability of the geometry and the charged distribution obtained from such spin contaminated wave functions is severely hampered.

Unrestricted Hartree–Fock (UHF) calculations on thiophene oligomer radical cations $n\mathrm{T}^{+\cdot}$ ($n = 2$, 4, 6, 8 and 10) were often affected by high spin contamination. Thus, in order to obtain reliable HF-level geometry and wave functions, the Restricted Open shell Hartree–Fock (ROHF) method has been used, which rules out spin contamination a priori [20].

DFT calculations were performed within the Unrestricted Kohn–Sham (UKS) scheme and were never seriously affected by spin contamination. The Becke + Lee–Yang–Parr (B-LYP) functional [21,22] has been used in all DFT calculations. B-LYP is a correlated functional with non-local gradient corrections and has been proven to be the non-hybrid functional with the best overall performance [23]. The same B-LYP functional has been used in our previous paper on doubly charged oligothiophenes [19].

All calculations have been performed using the 3-21G* basis set, which has been shown to produce reliable results for organo-sulphur molecular systems [24].

The geometry of $n\mathrm{T}^{+\cdot}$ oligomers was optimized under the C_{2h} symmetry constraint. The latter is a reasonable approximation since the charged portions of the polymer backbone undergo a quinoid distortion which increases the coplanarity of neighboring thiophene rings.

To investigate the energetics of aromatic vs. quinoid geometry in bithiophenes, RHF, B-LYP and MP2 [25] calculations have been performed using both the 3-21G* and the 6-31G* basis sets.

The Gaussian94 [26] system of programs has been used to carry out all calculations. An in-house modified version of the software package [27], with enhanced parallel performance, has been used on multiprocessor supercomputers such as the Cray-T3E (CINECA Supercomputing Center, Bologna) and the Convex-HP Exemplar X-Class (CILEA Supercomputing Center, Milano).

3. Results

We first present the optimized geometry of the $n\mathrm{T}^{+\cdot}$ ($n = 2$, 4, 6, 8 and 10) as computed at the ROHF/3-21G* and UBLYP/3-21G* levels. In particular, we focus our attention on the values of carbon–carbon and carbon–sulphur bond lengths along two paths in the oligomer skeleton: the C–C path (Fig. 2a) that involves only C–C bonds and the C–S path (Fig. 2b) involving only the C–S bonds. This latter path shows the behavior of the C–S bond length, which is seldom considered in this kind of investigations. In the second part of this section, we investigate the energetics of the neutral 2T using α,α′ disubstitution to force either the aromatic or the quinoid geometry on the system.

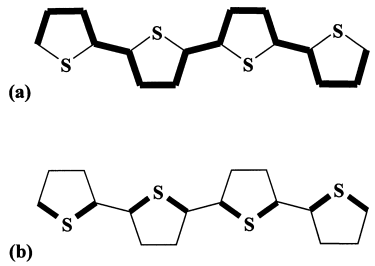

Fig. 2. The two paths used in this work to report and compare bond lengths computed at various levels of theory: (a) the C–C path, (b) the C–S path.

3.1. HF results on $nT^{+\cdot}$

In Fig. 3 are depicted (as open symbols) the optimized bond length along the C–C path for $n\mathrm{T}^{+\cdot}$ ($n = 4$, 6, 8 and 10) as computed at the ROHF/3-21G* level. There is a clear evidence of a quinoid-like distortion, with reversed bond length alternation, in the oligomers' backbone, which is localized over the two innermost thiophene rings. The innermost inter-ring bond shows a partial double bond character with a length of 1.390 Å, whereas the adjacent bond along the C–C path is slightly longer (1.400 Å). The spatial extension of the quinoidic defect does not change as the length of the oligomer increases. The boundary between the quinoid-like and the aromatic-like phases, characterized by opposite bond length alternation patterns, is located near bond number 3 as shown in Fig. 3. The outer rings of the higher oligomers are only slightly perturbed by the presence of the singly charged defect. They are characterized by the aromatic-like bond length alternation and their geometry is almost identical to the one found in the corresponding neutral oligomers optimized at the same level of theory [28]. Within the singly charged defect, the magnitude of the quinoid-like bond length alternation is about 0.02 Å. This is a value much smaller than both the aromatic bond length alternation of the neutral thiophene oligomers (0.06–0.08 Å) and the quinoidic bond length alternation within the bipolaronic defect in doubly charged oligomers $n\mathrm{T}^{2+}$ (0.08 Å) [19,29].

The carbon–sulphur bonds along the C–S path (Fig. 4, open symbols) show alternation of shorter and longer bonds around the average value found for the neutral oligomers (1.738 Å). Within each thiophene ring, the C–S bond nearest to the center of the oligomer is longer than the adjacent one.

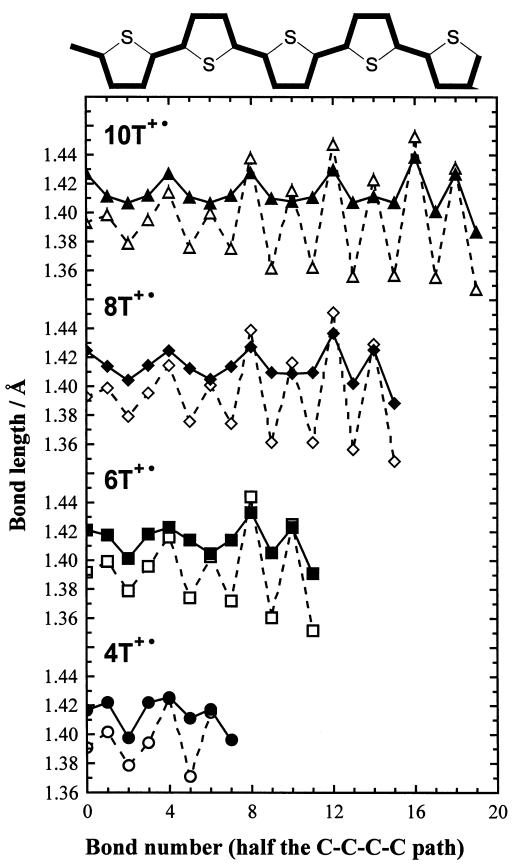

Fig. 3. Optimized bond lengths for half the C–C path of $n\mathrm{T}^{+\cdot}$ ($n = 4$, 6, 8 and 10) at the ROHF/3-21G* (open symbols) and UB-LYP/3-21G* (filled symbols) levels. The bond numbering is from the center towards one end of the oligomer.

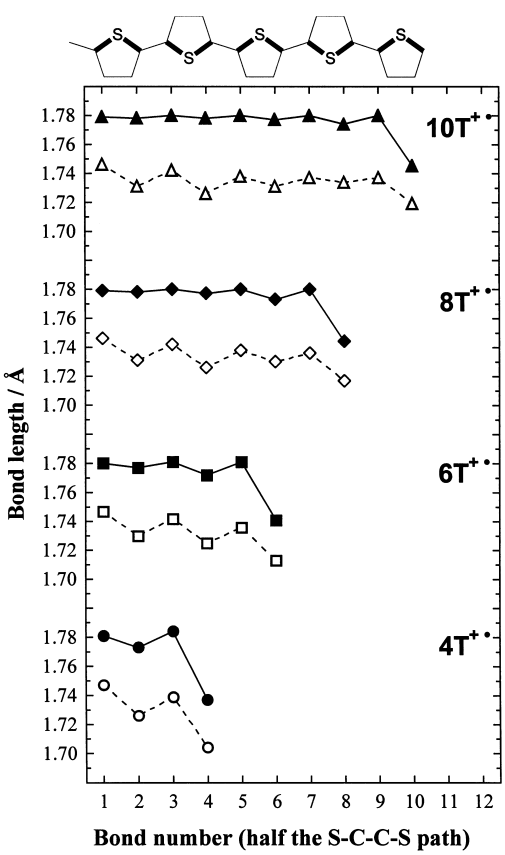

Fig. 4. Optimized bond lengths for half the C–S path of $n\mathrm{T}^{+\cdot}$ ($n = 4$, 6, 8 and 10) at the ROHF/3-21G* (open symbols) and UB-LYP/3-21G* (filled symbols) levels. The bond numbering is from the center towards one end of the oligomer.

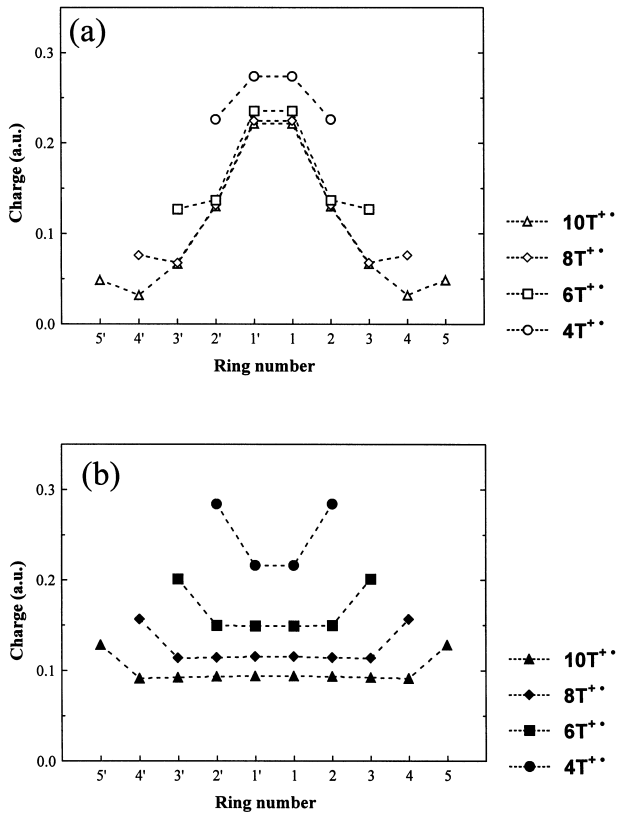

Fig. 5. Per-ring net charge profile for $n\mathrm{T}^{+\cdot}$ ($n = 4$, 6, 8 and 10) as computed at (a) the ROHF/3-21G* and (b) UB-LYP/3-21G* levels.

To quickly depict the electronic distribution, we use the per-ring net charge, which is the sum over the atoms belonging to each thiophene ring of the atomic charges as computed by the Mulliken population analysis of the density matrix. In the same way, we define the per-ring spin density from the spin density matrix. In Fig. 5a is reported the per-ring net charge profile of $n\mathrm{T}^{+\cdot}$ ($n = 4$, 6, 8 and 10) computed from the ROHF/3-21G* electronic density. The quinoidic structural distortion localized near the center of the oligomer chain finds its counterpart in the localization of a major percentage of the exceeding positive charge over the innermost thiophene rings.

A similar trend is observed for the per-ring spin density as computed at the ROHF/3-21G* level (Fig. 6a). [2] A more detailed analysis of the distribution of the unpaired electron for $10\mathrm{T}^{+\cdot}$ shows that it is mainly localized on the inner α carbons (0.117 a.u.), the inner β carbons (0.088 a.u.) and the outer α carbons (0.103 a.u.) of rings 1 and 1′.

3.2. DFT results on $n\mathrm{T}^{+\cdot}$

In Fig. 3 are depicted (as filled symbols) the optimized bond length along the C–C path for $n\mathrm{T}^{+\cdot}$ ($n = 4$, 6, 8 and 10) as computed at the UB-LYP/3-21G* level. The structure of the oligomer is uniformly modified by the presence of the singly charged defect, which is in fact fully delocalized. Only in the shortest oligomer $4\mathrm{T}^{+\cdot}$ a definite quinoid-like phase spans over the two innermost thiophene rings. In longer oligomers $n\mathrm{T}^{+\cdot}$ ($n = 6$, 8 and 10), the most relevant structural feature is the chain-end bond pattern whose shape remains qualitatively unchanged as the number of rings increases. Along the C–C path, the chain-end section is characterized by an aromatic-like bond length alternation of about 0.02 Å, which extends over five bonds. The average aromatic bond length alternation found in neutral oligomers at the B-LYP/3-21G* level is of 0.03 Å [28]. The inner portion of higher oligomer structure shows a bond length pattern which cannot be designated neither as aromatic-like nor as quinoid-like since there is no simple alternation of long and short C–C bonds. Moreover, no evidence of convergence towards a C–C bond length pattern of some distinct shape is evident; in fact, in the $6\mathrm{T}^{+\cdot}$ and longer oligomers, the structure of all, but the two outermost rings is continuously evolving.

The C–S bond lengths along the C–S path (Fig. 4, filled symbols) show a much smoother profile as compared to the values obtained at the ROHF/3-21G* level. As in the case of the C–C bonds, an evident chain-end effect is found, which spans over the two outermost rings and is unchanged as the length of the oligomer increases. In

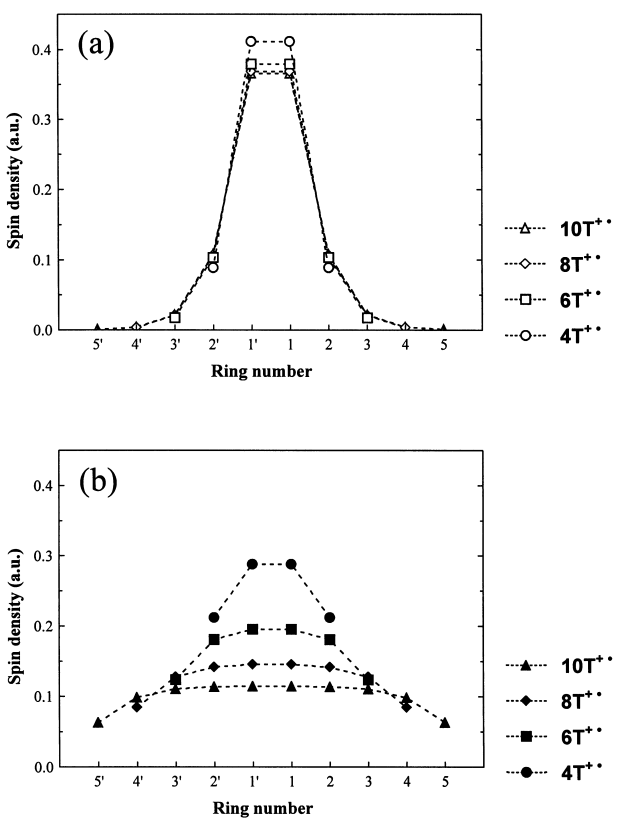

Fig. 6. Per-ring spin density profile for $n\mathrm{T}^{+\cdot}$ ($n = 4$, 6, 8 and 10) as computed at (a) the ROHF/3-21G* and (b) UB-LYP/3-21G* levels.

[2] Within the ROHF formalism, the spin density of a radical cation is given by the squared modulus of the singly occupied alpha molecular orbital, whereas in the UB-LYP framework, it is computed by subtracting the density of the beta electrons from the density of the alpha electrons.

particular, the two outermost bonds are significantly shorter than all the other C–S bonds by about 0.02 Å.

In Fig. 5b, the per-ring net charge profile of $n\mathrm{T}^{+\cdot}$ ($n = 4$, 6, 8 and 10) is reported as computed from the UB-LYP/3-21G* electronic density. The exceeding positive charge is evenly distributed on all the rings in the oligomers except the two outermost rings, which bear a larger amount of charge. These features follow the delocalized character of the structural distortion.

The per-ring spin density as computed at the UB-LYP/3-21G* level (Fig. 6b) (^{2}) is scattered uniformly over all rings in the oligomer, but contrary to what is observed for the charge excess, the two outermost rings carry a smaller amount of spin density. A more detailed analysis shows that the major contributions originate from carbon atoms. Moreover, being the per-ring spin density almost constant, all values over the inner rings fall into a narrow interval ($0.025 \div 0.035$ a.u.), whereas over the outermost rings, the range of spin density atomic contributions is larger ($-0.005 \div 0.05$ a.u.).

3.3. Calculations on neutral 5,5′-disubstituted 2T

By means of suitable 5,5′-disubstitutions, it is possible to induce either an aromatic or a quinoid geometry in the neutral 2T molecule. Fig. 7 shows the two substitutions patterns used for the present study, namely 5,5′-dimethyl-2,2′-bithiophene and 5,5′-dimethylen-2,2′-bithiophene.

The geometry of both compounds was optimized at the HF, B-LYP and MP2 level using the 3-21G* and the 6-31G* basis sets. The two-ring system was kept planar during the geometry optimization in order to investigate the energetics of the aromatic vs. quinoid structures within the same approximations previously used for the oligothiophene radical cations $n\mathrm{T}^{+\cdot}$.

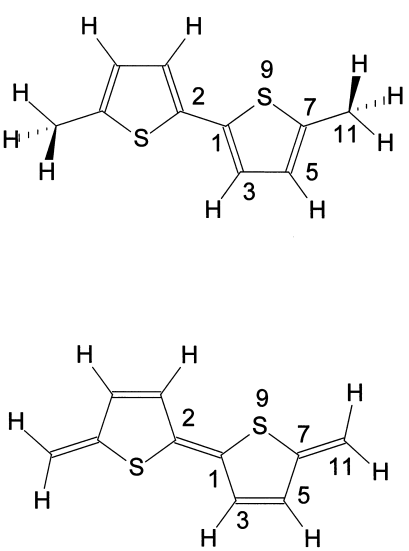

Fig. 7. Molecular structure of 5,5′-dimethyl-2,2′-bithiophene (top) and 5,5′-dimethylen-2,2′-bithiophene (bottom), with numbering used in Table 1.

Table 1
C–C and C–S bond lengths (in Å) of 5,5′-dimethyl and 5,5′-dimethylen-2,2′-bithiophene optimized at the HF/6-31G*, B-LYP/6-31G* and MP2/6-31G* levels. See Fig. 7 for the atoms numbering

Bond length/Å	5,5′-Dimethyl-2,2′-bithiophene			5,5′-Dimethylen-2,2′-bithiophene		
	HF/6-31G*	B-LYP/6-31G*	MP2/6-31G*	HF/6-31G*	B-LYP/6-31G*	MP2/6-31G*
C2–C1	1.462	1.451	1.446	1.333	1.381	1.368
C1–C3	1.351	1.391	1.385	1.462	1.444	1.438
C3–C5	1.433	1.428	1.412	1.328	1.370	1.358
C5–C7	1.346	1.382	1.374	1.466	1.455	1.449
C7–C11	1.505	1.512	1.498	1.323	1.360	1.349
S9–C1	1.742	1.779	1.733	1.781	1.805	1.770
S9–C7	1.735	1.768	1.727	1.779	1.810	1.774

The optimized C–C and C–S bond lengths of 5,5′-dimethyl and 5,5′-dimethylen-2,2′-bithiophene are collected in Table 1. As predictable, the methyl substituents do not modify the typical aromatic bond length alternation of the thiophene rings. The maximum difference between a short and long carbon–carbon bond is as large as 0.111 Å at the HF level, whereas when electron correlation effects are taken into account, it is reduced by about a half ($0.060 \div 0.061$ Å). The C–S bond lengths behave differently as either correlated method is used. At the B-LYP level, the C–S bonds are longer by about 0.03 Å with respect to the HF values, whereas at the MP2 level, they are slightly shorter. The same differences between the HF and the B-LYP geometry have been found also in longer oligomers [28]. The substitution by means of two methylene groups, forces the two-ring system to assume an inverted, quinoid-like bond length alternation (Table 1). The maximum difference between a short and long carbon–carbon bond becomes 0.138, 0.085 and 0.091 Å at the HF, B-LYP and MP2 levels, respectively. The C–S bond lengths in 5,5′-dimethylen-2,2′-bithiophene are longer with respect to what were found for the 5,5′-dimethyl substitution by $0.03 \div 0.04$ Å. However, the optimized values provided by the three theoretical methods follow the same trend.

4. Discussion

4.1. The discrepancy between HF and B-LYP results for the oligothiophene radical cations $nT^{+\cdot}$

Before discussing the details of the comparison between HF and DFT results, a methodological issue should be addressed about the comparison of results obtained by means of a restricted wave function (ROHF) with the ones from a unrestricted scheme (UB-LYP). We must point out that, apart from the restricted/unrestricted choice, there are other differences between ROHF and UB-LYP which are much more important. Indeed, the two methods are developed from different monoelectronic operators within

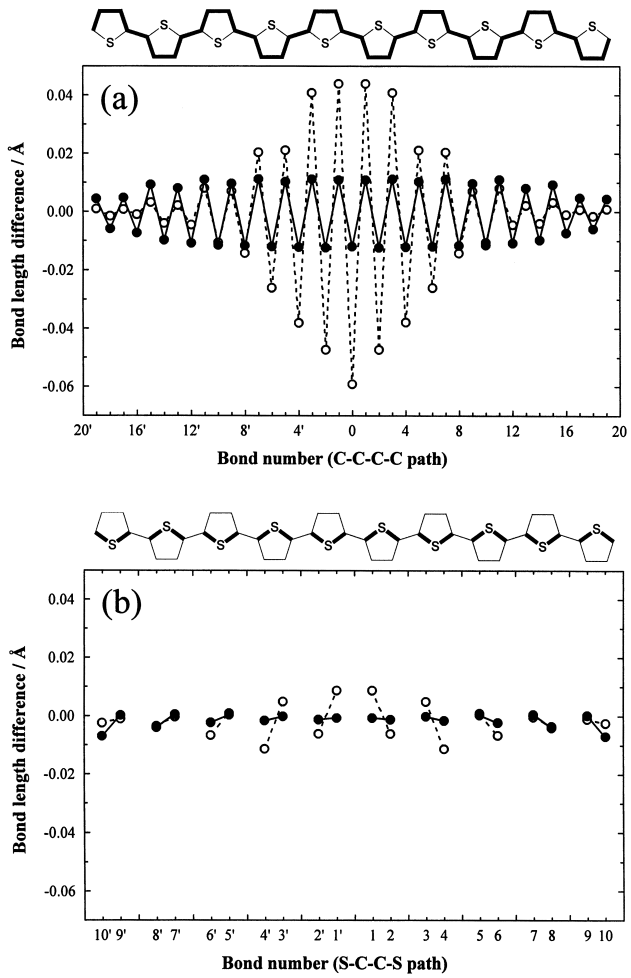

Fig. 8. Differences between corresponding bond lengths of $10T^{+\cdot}$ and 10T as computed at the HF/3-21G* (open symbols) and B-LYP/3-21G* (filled symbols) levels along (a) the C–C path and (b) the C–S path.

different theoretical frameworks [30]. The ROHF method includes the exchange energy in an exact way given the monodeterminantal character of the wave function, but does not take into account the electron correlation. On the other hand, the UB-LYP method includes the electron correlation effects, but the exchange energy is computed in a way that does not directly rely on the antisymmetry of the wave function.

In Fig. 8a, the differences between corresponding bond lengths along the C–C path of $10T^{+\cdot}$ and 10T are shown. [3] In this way, the net effect of the presence of the singly charged defect is made evident. The ROHF results (Fig. 8a, open symbols) are consistent with a localized character of the polaronic defect since the oligomer geometry is strongly perturbed only over the four innermost rings (up to -0.06 Å at the central inter-ring bond). Moving towards the chain ends, the perturbation with respect to the 10T geometry steeply decreases to negligible values over the two outermost rings. On the other hand, the UB-LYP results (Fig. 8a, filled symbols) show a fully delocalized singly charged defect. All the C–C bond lengths are uniformly modified with respect to the neutral structure: the long bonds (inter-ring bonds and β–β bonds) are shortened by 0.02 Å, while the length of the short ones (α–β bonds) is increased by the same amount. Only slightly smaller changes in the C–C bonds are found over the chain-end rings.

Similar considerations can be made on the differences between the lengths of corresponding C–S bonds in the neutral and the singly charged oligomers. The values optimized at the ROHF/3-21G* level (Fig. 4, open symbols) change significantly only for the four innermost rings, up to a maximum difference of about 0.02 Å. On the contrary, the C–S bond lengths optimized at the UB-LYP/3-21G* level (Fig. 4, filled symbols) show noticeable changes with respect to the corresponding *n*T (up to 0.008 Å) only for the two outermost bonds of the chain-end rings. This is

[3] The values of the geometric parameter of the neutral 10T have been extrapolated from the optimized structures of 8T by replicating the two innermost rings.

consistent with the fact that, at the UB-LYP/3-21G* level, the chain-end rings carry a portion of the positive charge larger than the other thiophene rings in the oligomer.

4.2. The energetics of aromatic vs. quinoid geometry for the neutral 2T systems

According to the widely accepted theory [7] of topological defects in non-degenerate conjugated system, the per-ring energy difference between the aromatic and the quinoid structure is responsible for the confinement of a soliton pair to form a singly charged polaron or a doubly charged bipolaron. The larger is this energy difference, the smaller is the spatial extension of the defect.

To provide an explanation of the discrepancy between the HF and the B-LYP results described in the previous section, we evaluate the energy difference between the aromatic and the quinoid geometries in the neutral polythiophene chain using bithiophene as model compound. The structural parameters for aromatic and quinoid geometries, were taken from 5,5′-dimethyl 2T and 5,5′-dimethylen 2T, respectively (Table 1). The model bithiophenes were assumed planar and all C–H bond lengths were fixed to 1.08 Å. In Table 2 are reported the ab initio energy values for the aromatic and the quinoid structures of 2T, as computed at the HF, B-LYP and MP2 levels of theory using the 6-31G* basis set. These results clearly show how the electron correlation strongly reduces (from 45 to about 14 kcal mol^{-1}) the energy difference between the aromatic and the quinoid geometry.

The electronic structure of the oligothiophenes radical cation $n\mathrm{T}^{+\cdot}$ is obviously perturbed by the removal of an electron and a large relaxation takes place. However, even for the simplest model system (the neutral 2T), HF and B-LYP provide markedly different estimations of the energy required to turn the aromatic geometry of the thiophene ring into quinoid. Thus, the qualitatively discrepancies found for the geometry and charge distribution of the radical cations $n\mathrm{T}^{+\cdot}$, are not related to the specific molecular systems being considered, but rather to the theoretical methods. The positive charge and the size of the oligothiophenes simply magnify this fundamental discordance.

The MP2 method takes into account the electron correlation on a completely independent basis with respect to B-LYP, but it essentially confirms all the results of the DFT approach. However, the MP2 method cannot be readily applied to compute the optimized geometry and the charge distribution of large oligothiophenes radical cation $n\mathrm{T}^{+\cdot}$, because of the N^4 scaling of its computational cost.

Table 2
Ab initio energy values for neutral bithiophene 2T as computed at the HF, B-LYP and MP2 levels of theory, assuming the aromatic (5,5′-dimethyl 2T) and quinoid (5,5′-dimethylen 2T) geometry

	Energy/Hartree		ΔE/ kcal mol^{-1}
	Aromatic geometry	Quinoid geometry	
HF/6-31G*	−1101.42908	−1101.35679	45.4
B-LYP/6-31G*	−1104.64437	−1104.62360	13.0
MP2/6-31G*	−1102.76674	−1102.74206	15.5

5. Conclusion

Oxidized thiophene oligomers are object of remarkable research efforts as they represent model compounds for the charge defects in polythiophenes. In this contribution, we reported a theoretical modeling of the structural and electronic properties of a series of oligothiophenes radical cations $n\mathrm{T}^{+\cdot}$ ($n = 2$, 4, 6, 8 and 10).

The optimized geometry, charge and spin density distributions calculated at the ROHF/3-21G* are consistent with the formation of a localized charge defects characterized by a quinoid structural distortion over the two innermost thiophene rings. By introducing the effects of the electron correlation within the framework of the DFT at the UB-LYP/3-21G* level, the shape of the charge defect changes becoming fully delocalized. The excess of positive charge is evenly distributed over the whole length of the oligomer and the structure of all rings changes in a similar way preventing the formation of any localized structural defect. The serious disagreement between the outcome of HF and B-LYP calculations already reported for doubly charged oligothiophenes [19] is here established also in the case of singly charged systems.

The energetics of the aromatic vs. quinoid geometry in the neutral polythiophene chain has been investigated using neutral 2T as model compound. By taking into account the electron correlation, either by means of the B-LYP or the MP2 method, the energy required to turn the aromatic geometry into quinoid, is strongly reduced with respect to the estimation provided by the HF approach. This suggests that the qualitative discrepancies found between HF and B-LYP results for charged oligothiophenes, are essentially due to electron correlation effects and not to the actual molecular system being under investigation.

Further calculations are in progress to assess the reliability of B-LYP by comparison with both other functionals and post-HF perturbative methods. Finally, the effects of charge screening by effective counterions on the results of the different theoretical approaches will be investigated in future papers.

Acknowledgements

Financial support from the Italian National Research Council, C.N.R. (Progetto Finalizzato Materiali Speciali per Tecnologie Avanzate — MSTA2 and Grants

97.00506.CT11 and 98.00651.CT11) as well as computational support by CILEA (Milano) and CINECA (Bologna) supercomputing centers are gratefully acknowledged.

References

[1] T.A. Skotheim (Ed.), Handbook of Conducting Polymers, Vols. 1–2, Marcel Dekker, New York, 1986.
[2] J.-L. Brédas, R. Silbey (Eds.), Conjugated Polymers: The Novel Science and Technology of Highly Conducting and Nonlinear Optically Active Materials, Kluwer Academic Publishing, Netherlands, 1991.
[3] J. Roncali, Chem. Rev. 92 (1992) 711.
[4] R.L. Elsenbaumer, K.Y. Jen, R. Oboodi, Synth. Met. 15 (1986) 169.
[5] T.-C. Chung, J.H. Kaufman, A.J. Heeger, F. Wudl, Phys. Rev. B 30 (1984) 702.
[6] Z. Vardeny, E. Ehrenfreund, O Brafman, M. Nowak, H. Schaffer, J.A. Heeger, F Wudl, Phys. Rev. Lett. 56 (1986) 671.
[7] J. Heeger, S. Kivelson, J.R. Schrieffer, W.-P. Su, Rev. Mod. Phys. 60 (1988) 781.
[8] D. Bertho, C. Jouanin, Phys. Rev. B 35 (1987) 626.
[9] D. Bertho, A. Laghddir, C. Jouanin, Phys. Rev. B 38 (1988) 12531.
[10] Y. Furakawa, Synth. Met. 69 (1995) 629.
[11] M.G. Hill, K.R. Mann, L.L. Miller, J.F. Penneau, J. Am. Chem. Soc. 114 (1992) 2728.
[12] J.A.E.H. van Haare, E.E. Havinga, J.L.J. van Dongen, R.A.J. Janssen, J. Cornil, J.L. Brédas, Chemistry: A European Journal 4 (1998) 1509.
[13] M.A. Sato, M. Hiroi, Synth. Met. 69 (1995) 307.
[14] Nessakh, G. Horowitz, F. Garnier, F. Deloffre, P. Srivastava, A. Yassar, J. Electroanal. Chem. 399 (1995) 97.
[15] M.G. Hill, J.F. Penneau, B. Zinger, K.R. Mann, L.L. Miller, Chem. Mater. 4 (1992) 1106.
[16] B. Zinger, K.R. Mann, M.G. Hill, L.L. Miller, Chem. Mater. 4 (1992) 1113.
[17] N. Yokonuma, Y. Furukawa, M. Tasumi, M. Kuroda, J. Nakayama, Chem. Phys. Lett. 255 (1996) 431.
[18] Y. Furakawa, J. Phys. Chem. 100 (1996) 15644.
[19] G. Moro, G. Scalmani, U. Cosentino, D. Pitea, Synth. Met. 92 (1998) 69.
[20] J.S. Binkley, J.A. Pople, P.A. Dobosh, Mol. Phys. 28 (1974) 1423.
[21] D. Becke, Phys. Rev. A 38 (1988) 3098.
[22] Lee, W. Yang, R.G. Parr, Phys. Rev. B 37 (1988) 785.
[23] G. Johnson, P.W. Gill, J.A. Pople, J. Chem. Phys. 98 (1993) 5612.
[24] G. Moro, G. Scalmani, U. Cosentino, D. Pitea, J. Mol. Struct.: THEOCHEM 366 (1996) 43.
[25] A. Szabo, N.S. Ostlund, Modern Quantum Chemistry, McGraw-Hill, New York, 1989.
[26] M.J. Frisch, G.W. Trucks, H.B. Schlegel, P.M.W. Gill, B.G. Johnson, M.A. Robb, J.R. Cheeseman, T. Keith, G.A. Petersson, J.A. Montgomery, K. Raghavachari, M.A. Al-Laham, V.G. Zakrzewski, J.V. Ortiz, J.B. Foresman, J. Cioslowski, B.B. Stefanov, A. Nanayakkara, M. Challacombe, C.Y. Peng, P.Y. Ayala, W. Chen, M.W. Wong, J.L. Andres, E.S. Replogle, R. Gomperts, R.L. Martin, D.J. Fox, J.S. Binkley, D.J. Defrees, J. Baker, J.P. Stewart, M. Head-Gordon, C. Gonzalez, J.A. Pople, Gaussian 94, Revision E.2, Gaussian, Pittsburgh, PA, 1995.
[27] G. Scalmani, G. Moro, U. Cosentino, D. Pitea, Parallel execution of Gaussian94 using P.V.M. and M.P.I. as message passing tools, III National Congress of Computer Science in Chemistry, Naples, February, 27th–March, 1st 1997.
[28] G. Scalmani, G. Moro, U. Cosentino, D. Pitea, unpublished results.
[29] Ch. Ehrendorfer, A. Karpfen, J. Phys. Chem. 98 (1994) 7492.
[30] J. Baerends, O.V. Gritsenko, J. Phys. Chem. A 101 (1997) 5383.